



Die Grenzen der  
Chemie neu ausloten?  
It takes  
#HumanChemistry

Wir suchen kreative Chemikerinnen und Chemiker,  
die mit uns gemeinsam neue Wege gehen wollen –  
mit Fachwissen, Unternehmertum und Kreativität für  
innovative Lösungen. Informieren Sie sich unter:

[evonik.de/karriere](https://www.evonik.de/karriere)

# Compartmentalized Jet Polymerization as a High-Resolution Process to Continuously Produce Anisometric Microgel Rods with Adjustable Size and Stiffness

Andreas J. D. Krüger, Onur Bakirman, Luis P. B. Guertzoni, Alexander Jans, David B. Gehlen, Dirk Rommel, Tamás Haraszti, Alexander J. C. Kuehne, and Laura De Laporte\*

In the past decade, anisometric rod-shaped microgels have attracted growing interest in the materials-design and tissue-engineering communities. Rod-shaped microgels exhibit outstanding potential as versatile building blocks for 3D hydrogels, where they introduce macroscopic anisotropy, porosity, or functionality for structural guidance in biomaterials. Various fabrication methods have been established to produce such shape-controlled elements. However, continuous high-throughput production of rod-shaped microgels with simultaneous control over stiffness, size, and aspect ratio still presents a major challenge. A novel microfluidic setup is presented for the continuous production of rod-shaped microgels from microfluidic plug flow and jets. This system overcomes the current limitations of established production methods for rod-shaped microgels. Here, an *on-chip* gelation setup enables fabrication of soft microgel rods with high aspect ratios, tunable stiffness, and diameters significantly smaller than the channel diameter. This is realized by exposing jets of a microgel precursor to a high intensity light source, operated at specific pulse sequences and frequencies to induce ultra-fast photopolymerization, while a change in flow rates or pulse duration enables variation of the aspect ratio. The microgels can assemble into 3D structures and function as support for cell culture and tissue engineering.


Anisometric microscale building blocks play an important role in many applications to program the mechanical, optical, electronic, and thermal properties of the resulting composite material. These anisometric colloidal entities exhibit outstanding self-assembly behavior including shape specific organization<sup>[1]</sup> and inter-particle interactions.<sup>[2–4]</sup> Recently, anisotropy and the mechanical properties of microgels and particles have gained significant attention in the fields of drug delivery and tissue engineering.<sup>[5]</sup> In the case of drug delivery, particle size and shape have a substantial impact on cellular uptake, circulation in the blood, and distribution in biological systems.<sup>[6,7]</sup> For tissue engineering, *bottom-up* approaches use particle self-assembly and self-organization to fabricate and organize microgels into 3D macroscopic scaffolds.<sup>[5,8–10]</sup> Recently, our research group introduced the Anisogel that induces mechanical and structural anisotropy to guide cells and regenerating nerves in a unidirectional manner.<sup>[11–13]</sup> Alternatively, others have

incorporated gold nanoparticles inside anisometric microgels made from thermoresponsive polymers to achieve actuation upon light exposure.<sup>[14,15]</sup> In parallel, we developed a microfluidic plug flow Michael-type addition-based gelation system that enables continuous production of large rod-shaped microgels loaded with cells. To maintain high cell viability during gelation, the crosslinking chemistry, the stiffness of the generated microgel, and its degradation play crucial roles.<sup>[16]</sup> Inspired by these studies, there arises an increasing demand of functional anisometric building blocks for novel high-performance materials and new fabrication methods with high-throughput yield, while balancing four specific process parameters: particle size, particle anisotropy and aspect ratio, production rate, and the mechanical properties of the material. Currently, the generation of anisometric particles is performed using either batch or continuous production techniques. While batch processes allow for the production of polymer particles or microgels with high anisotropy and feature sizes below 100 nm for a wide range of materials, they require multi-step processing, which severely limits production rates. Established batch protocols

A. J. D. Krüger, O. Bakirman, L. P. B. Guertzoni, A. Jans, D. B. Gehlen, D. Rommel, Dr. T. Haraszti, Prof. A. J. C. Kuehne, Prof. L. De Laporte  
DWI – Leibniz Institute for Interactive Materials  
52074 Aachen, Germany  
E-mail: delaporte@dwi.rwth-aachen.de

Prof. A. J. C. Kuehne  
Institute of Organic and Macromolecular Chemistry  
Ulm University  
89081 Ulm, Germany

Prof. L. De Laporte  
Lehrstuhl für Textilchemie und Makromolekulare Chemie  
52056 Aachen, Germany

 The ORCID identification number(s) for the author(s) of this article can be found under <https://doi.org/10.1002/adma.201903668>.

© 2019 DWI – Leibniz Institute for Interactive Materials. Published by WILEY-VCH Verlag GmbH & Co. KGaA, Weinheim. This is an open access article under the terms of the Creative Commons Attribution-NonCommercial-NoDerivs License, which permits use and distribution in any medium, provided the original work is properly cited, the use is non-commercial and no modifications or adaptations are made.

DOI: 10.1002/adma.201903668

include template-based gelation systems, first published by DeSimone et al. as particle replication in non-wetting templates (PRINT).<sup>[4,11,17–20]</sup> Alternatively, particle deformation can be employed using strategic shearing or heating of solid polymer spheres resulting in ellipsoidal nano- or microparticles.<sup>[2,21,22]</sup>

Continuous microfluidic flow systems can overcome the low production rates of batch processes. Here, (pre-)polymer containing elongated plugs are generated by operating T-junctions,<sup>[23]</sup> cross-junctions,<sup>[16]</sup> or flow-focusing devices<sup>[24]</sup> in the dripping or plug flow regime.<sup>[25]</sup> The precursor solution inside these microfluidic plugs can be polymerized rapidly on chip via photoinitiation, resulting in covalently crosslinked disk or rod-shaped gels and particles.<sup>[23,24]</sup> Alternatively, noncovalent crosslinking can be triggered by calcium or temperature in the case of alginates<sup>[26]</sup> or gelatin,<sup>[10]</sup> respectively, or two-component covalent Michael-type addition can be employed to produce cell-loaded soft microgel rods.<sup>[10,16]</sup> Furthermore, microfluidic plug flow was utilized to obtain plug microreactors, in which solid anisometric nanocrystals were synthesized.<sup>[27]</sup> Alternatively, parallel flows in microfluidic were utilized to produce continuous microfibers from an alginate precursor solution, crosslinked via calcium.<sup>[28]</sup> In order to discontinue a jet, consisting of 54 wt% poly(ethylene glycol) diacrylate (PEG-DA) and photoinitiator, mechanical disruption via valve actuation was compared with pulsed light. This demonstrated that the pulsed light led to highly irregular and nonuniform fibers with lengths over 1 mm and one end being curled and bifurcated. The smallest obtained diameter using this technique was  $\approx 30 \mu\text{m}$  using a  $300 \mu\text{m}$  wide polydimethylsiloxane (PDMS) chip.<sup>[29]</sup>

Overall, anisometric particles produced in the dripping or plug flow regimes always exhibit the following three drawbacks: 1) the nonswollen diameter of particles is mostly equal to the channel diameter, with a minimal reported diameter of  $20 \mu\text{m}$ ,<sup>[30]</sup> 2) particle and microgel shapes are limited to disk and rod-shapes, and 3) most produced anisometric microgels are relatively stiff due to the high pre-polymer concentration required to achieve rapid *on-chip* crosslinking. As a solution for the last challenge, soft, biocompatible, rod-shaped microgels have recently been prepared on chip at polymer concentrations down to 2 wt% PEG (atomic force microscopy (AFM) *E*-modulus of 1.8 kPa) via a Michael-type addition of two components using a second inlet to increase pH and therefore the reaction rate.<sup>[16]</sup> To overcome limitations in shape anisometry/versatility and size, a technology called continuous flow lithography (CFL) was developed by Doyle et al., where photolithography is applied on a flowing stream of pre-polymer solution inside a microfluidic channel.<sup>[31]</sup> However, production rates of CFL are limited due to a tradeoff between spatial resolution and high flow rates. Stop flow lithography (SFL)<sup>[32]</sup> and modifications of this process<sup>[30,33–36]</sup> overcome this restriction by alternating between stopping the flow while the illumination takes place and flushing out of product. This technique gave rise to great advancements in this field and enables high-throughput production of particles with minimum sizes of  $2.5 \mu\text{m}$ .<sup>[32]</sup> However, the minimum possible feature size on transparency photomasks, as well as the decreasing depth of field with higher magnification objectives, inhibits the scope of this technique.

Characteristically, it is possible to either produce microgels with high resolution, i.e., small sizes at high precision

but low-throughput (e.g., PRINT, SFL), or at high-throughput where particle size and dispersity increase and aspect ratio deteriorates (plug flow droplet microfluidics, jet disruption, CFL). Therefore, current methods only cover a small area of the described parameter space, meaning they either deliver precise geometries or small size or operate at high-throughput (see Figure 1a). To extend the fields of application for rod-shaped microgels and produce these building blocks at industrially relevant scales, new processes are required.

Here, we develop a method, where we generate anisometric microgels, by segmented illumination of a microgel precursor stream and operating a microfluidic chip in the jetting regime. This microfluidic jet method overcomes current limitations and allows for the production of small (down to 10% of the channel diameter), anisometric microgels with precisely tunable aspect ratios at high flow rates and therefore high production rates. The versatility realized with this system is, unmet by any other method established so far, presenting a significant advancement in the production of anisometric microgels and particles.

We apply microfluidic flow-focusing devices, where an inner phase carrying the microgel precursor meets the outer phase at a four-way intersection. This device is produced by soft-lithography in silicone (PDMS), which is sealed using a microscopy glass slide. Access to the channels is provided by punching through the PDMS slab and connecting to polyethylene tubing. A microfluidic PDMS chip with a channel diameter of  $80 \mu\text{m}$  is employed throughout all experiments. The PDMS of the chip is stained with a red dye to prevent any waveguiding of light to areas in the chip where irradiation is not desired (details in Chapter 6.1, Supporting Information). The flow rates are adjusted so that the device runs in the plug flow regime or in the jetting regime.

The inner phase consists of PEG-DA ( $700 \text{ g mol}^{-1}$ ) in the presence of a water-soluble initiator lithium phenyl-2,4,6-trimethylbenzoyl-phosphinate (LAP) to facilitate a rapid gelation. The continuous phase consists of paraffin and surfactant in the case of plug flow gelation and pure Span80 for jet gelation. For photoinitiation of the crosslinking polymerization, a laser/UV-LED (light-emitting diode) driver unit is applied (Chapter 3 and Figure S1, Supporting Information) to control the power, frequency (up to 7 kHz), and duty cycle of the irradiation pulses. The stand-alone laser/UV-LED driver unit consists of an Arduino Uno microcontroller capable of outputting a pulse width modulation type signal, an amplification stage to increase the current up to 1 A, and a display/keypad shield to set the desired parameters (Figure S2, Supporting Information). Three different operation modes are available: a “continuous” mode, which provides a constant signal, a “single pulse” mode, which generates a pulse with defined duration, and a “steady pulse” mode, generating a pulse sequence of variable duty cycle and frequency. The device is coupled to a 365 nm UV-LED for microfluidic plug flow gelation experiments (Figure 1c) or a 405 nm single mode laser diode for jet gelation experiments (Figure 1d). The respective light sources are mounted to the glass side of the chip to irradiate the designated channel section.

In the case of plug flow gelation, the inner aqueous phase containing the pre-polymer is emulsified in a nonpolar paraffine oil phase with 2% ABIL EM 90 surfactant. The inner phase is separated into anisometric plugs of variable lengths as controlled by the flow rates and crosslinked while transiting



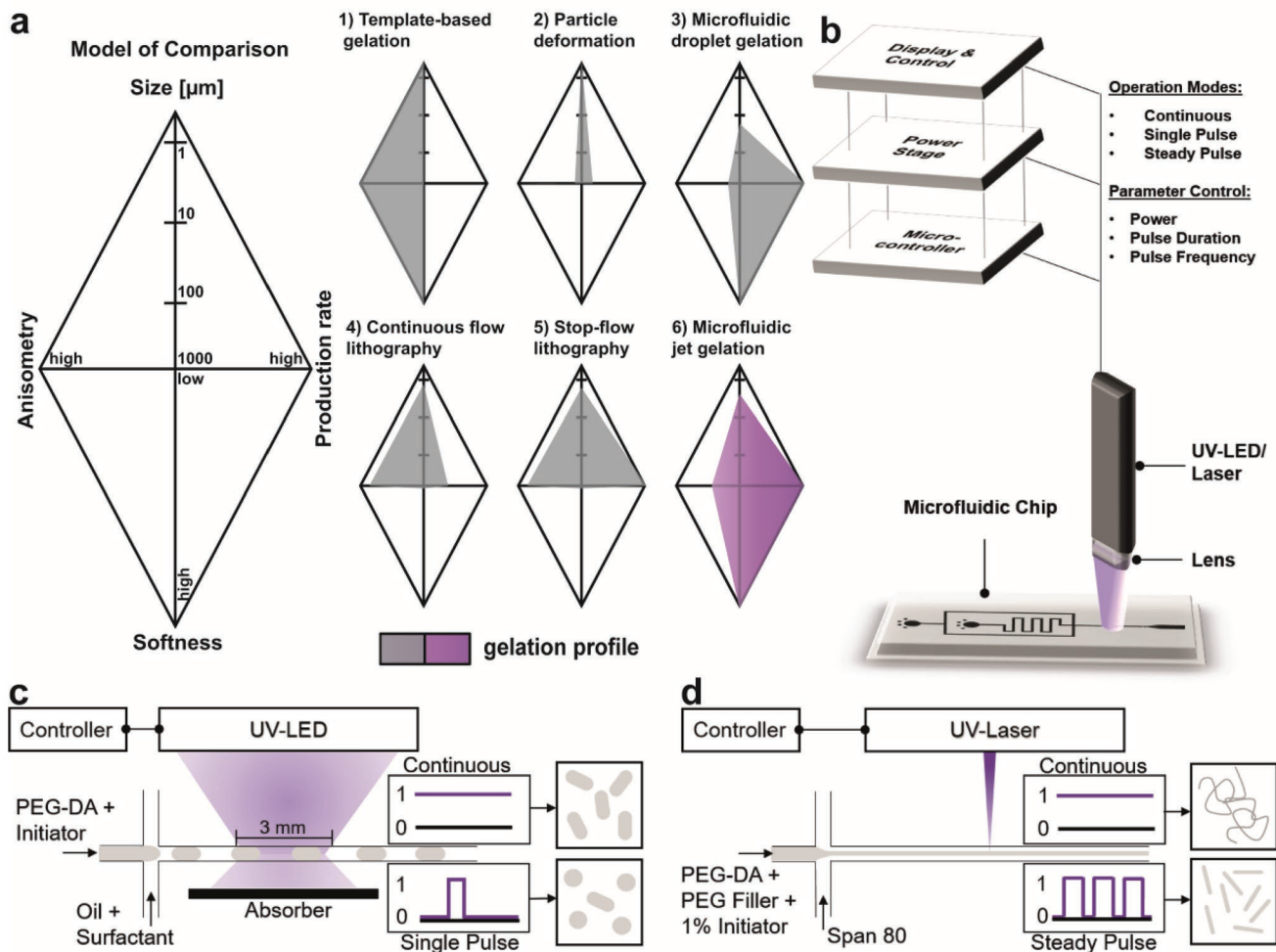


**Figure 1.** a) Fabrication methods to produce anisometric microgels and particles are characterized in parameter charts summarizing the capabilities and drawbacks of every method. Gray/violet areas describe accessible parameter combinations, whereas the white area displays conditions not realizable by the specific method. b) Schematic of microfluidic setup employed in this report: stand-alone laser/UV-LED driver unit with custom design to control operation (Chapter 3, Supporting Information). c) Schematic of microfluidic setup for *on-chip* plug flow gelation with an UV-LED operating in continuous or single pulse mode. Here, anisometric microgel rods are produced with diameters equal to the channel diameter, which further swell upon contact with water. Single pulse experiments are utilized to quantify gelation times. d) Schematic of microfluidic *on-chip* jet-gelation setup. A laser is operating in continuous mode to produce soft flexible microgel fibers with a diameter equal to the jet diameter. Pulsed laser light realizes compartmentalized gelation, leading to soft microgel rods with a diameter equal to the jet diameter. In both cases, swelling occurs upon contact with water, depending on the polymer composition.

the illuminated section of the channel. The degree of gelation is tuned by the intensity of the UV-LED and the irradiation time. As the spherical shape of the droplets is thermodynamically favored, the degree of gelation must be sufficiently high to fix their elongated rod-shape. Interestingly, this phenomenon can also be used to investigate the gelation kinetics when making use of the “single pulse” mode. The duration of the single pulse is gradually increased up to the point, at which the crosslinked microgel maintains its anisometric shape. Therefore, this minimal pulse duration represents the characteristic gelation time for a specific polymer composition. For this experiment to work, the flow rate has to be adjusted to the chosen pulse duration to ensure that the plug remains sufficiently long in the illumination spot. The plug generation frequency is so high that multiple rods are illuminated at once by the UV-light spot with a diameter of 3 mm. Depending on the PEG-DA concentration, minimum gelation times between 1.7 and 124 ms are

determined, while the highest polymer concentrations crosslink most rapidly (Figure 2a). These single pulse experiments represent a facile and fast method to precisely analyze gelation kinetics in confined microscale volumes, opening up new possibilities to characterize different light-induced crosslinking chemistries in gelling material systems.

We generate large amounts of microgel rods from different pre-polymer concentrations by continuous illumination of the pre-polymer solution plugs in the channel and their mechanical properties are analyzed. Swelling experiments reveal an increased diameter of approximately 29  $\mu\text{m}$  (36% increase compared to the channel diameter) in the case of 10 wt% PEG-DA, while 50 wt% pre-polymer microgels increase in diameter with 3  $\mu\text{m}$  (4% increase compared to the channel diameter) (Figure 2b). In fact, we are able to collect microgels at PEG-DA concentrations down to 9 wt% at the described gelation conditions; however, microgels prepared from 10 wt% of PEG-DA

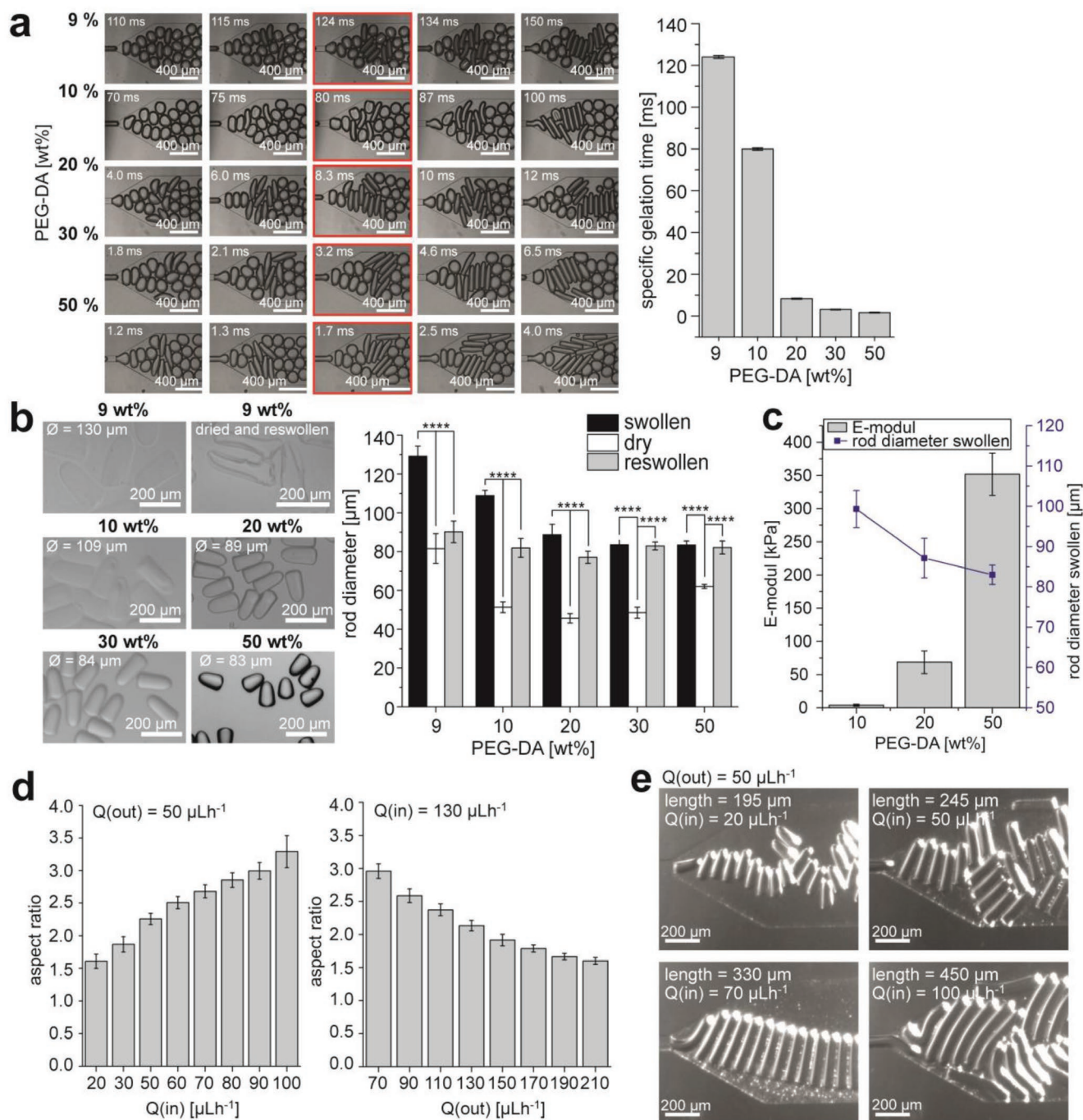


**Figure 2.** On-chip plug flow gelation is realized with a 365 nm UV-LED operating at a current up to 700 mA in either “single pulse” or “continuous” mode. The outer phase consists of paraffine oil with 2 wt% ABIL EM 90 surfactant. The inner phase contains PEG-DA at indicated concentrations and 1 wt% LAP in water. Microgels are collected in an ascorbic acid/ethanol solution to quench the polymerization and prevent off-chip gelation. The product is purified by repetitive centrifugation/decantation in heptane, isopropanol, and water. The microgels are characterized in their swollen state. All experiments are repeated at least three times. a) Brightfield microscopy images from the output of the microfluidic channel during single pulse experiments to monitor and determine the minimum pulse duration required for sufficient gelation to maintain a rod-shaped microgel without partial relaxation. Images depicting the specific gelation times are highlighted by a red frame. b) Microgel swelling significantly changes according to the PEG-DA concentration (in wt% as indicated) where microgels generated from lower pre-polymer concentrations exhibit a higher degree of swelling. The samples are monitored using brightfield microscopy after sedimentation on a glass slide. The diameters of the microgels are measured in the swollen, dried, and reswollen state for different polymer concentrations. c) The microgel stiffness is determined for different PEG-DA concentrations via AFM. d) Aspect ratios of rods with 10 wt% PEG-DA are altered by either changing  $Q_{in}$  at constant  $Q_{out}$  or vice versa. e) A wide range of short microgels (150 μm) to flexible long rods (up to 1 mm) is realized with reducing production rates for longer microgels.

or lower are irreversibly deformed after drying and reswelling. This deformation is likely due a lack of crosslinks and therefore absent restoring force to retain the microgel shape. The microgels, prepared at higher PEG-DA concentrations, re-swell in a reversible manner, indicating a stable crosslinked structure. AFM measurements elucidate that soft microgels with a PEG-DA concentration of 10 wt% have a Young's modulus ( $E$ -modulus) of 3.9 kPa, while for 50 wt% PEG-DA, a modulus of 352 kPa is realized. These results support the hypothesis of the higher network restoring force for more densely crosslinked microgels (Figure 2c).

To manipulate the microgel length and aspect ratio in the case of 10 wt% PEG-DA, the flow ratio of the inner to the outer phase is varied. Within the range of tested flow rates, a linear dependency between the increasing flow rate of the inner phase ( $Q_{in}$ ) and rod length is observed (Figure 2d). This relation is inverted in the case of a constant  $Q_{in}$ , while increasing the flow rate of the outer phase ( $Q_{out}$ ). The manipulation of the flow rates leads to a large variation of microgel aspect ratios ranging from short microgels (150  $\mu\text{m}$ ) to long and flexible rods up to a length of 450  $\mu\text{m}$  (Figure 2e).

Having developed a very rapid microgel precursor gelation system, we aim to further overcome the dimensional limits of the *on-chip* microgel production process. Therefore, we apply high intensity segmental gelation to a microfluidic device operated in the jetting regime. In contrast to the plug flow regime, where each plug is regarded as an individual and isolated template for each microgel, a jet represents a continuous system, where the isolation has to be induced by a pulsed illumination source. Beneficially, the diameter of a microfluidic jet can be significantly smaller than the width of the microfluidic channel and this diameter is adjustable by changing the flow ratio.<sup>[37]</sup> Jets in microfluidics have previously been applied to produce long hydrogel fibers;<sup>[38]</sup> however, they have never been utilized to generate short anisometric microgels. To widen the parameter space in which jet formation is possible and to stabilize the jet toward external influences, such as pressure fluctuations, the viscosity of the PEG-DA phase is raised by adding 2.4 wt% PEG (400.000  $\text{g mol}^{-1}$ ) and the outer phase is exchanged to pure Span80 to reduce the interfacial tension. While continuous irradiation of the 20 wt% PEG-DA jet produces an endless, soft hydrogel fiber sixfold thinner than the channel diameter (Figure 3a.1), we here make use of a novel strategy with a pulsed laser to produce microgel rods. A laser is preferred over an LED because of its higher intensity and the ability to focus the beam to small spot sizes. We apply LAP as the photoinitiator, enabling initiation with widely available 405 nm laser diodes, due to its considerable absorbance at this wavelength.<sup>[39]</sup>

The "steady pulse" mode yields crosslinked (irradiated) and noncrosslinked (not irradiated) sections of the jet. During pulsing, the jet is not destabilized and does not collapse into droplets; however, a modulation of the jet thickness becomes apparent (Figure 3a.2). This modulation may be explained by shrinking and a change in osmotic pressure as a result of the network formation. Toward the outlet, where the channel widens, the filament breaks up into segments, where the crosslinked sections represent the anisometric microgels and the noncrosslinked sections relax to droplet shapes. This

automatic separation occurs due to the abrupt drop of the flow velocity upon widening of the channel, promoting the separation of the inner phase into the crosslinked microgels and the remaining noncrosslinked pre-polymer solution (Figure 3a.2,3). At low pre-polymer concentrations of 10 or 20 wt% PEG-DA, the microgel compartments inside the transitioning jet fold, while an increase of the polymer concentration to 50 wt% PEG-DA yields significantly stiffer rods, which remain extended (Figure 3a.3 and Movie provided in the Supporting Information). AFM measurements confirm these observations, as a 20 wt% pre-polymer concentration yields microgels with an  $E$ -modulus of 5.5 kPa and 50 wt% leads to a modulus of 92 kPa (Figure 3c). Interestingly, jet derived microgels are significantly softer in comparison to rods, crosslinked in the plug flow system, which results from the combination of short exposure times in a high velocity jetting system.

To characterize the microfluidic jet, its velocity and diameter are measured as a function of the flow rates (Figure 3d). Blue latex beads ( $\varnothing = 800 \text{ nm}$ ) are added to the inner phase and tracked using a high-speed camera, recording 1000 frames per second. The velocity of the jet is obtained by tracing the travel distance of the beads over a defined period of time. Stable jets are realized at inner flow rates  $Q_{in}$  of 10, 20, and 30  $\mu\text{L h}^{-1}$  and outer flow rates  $Q_{out}$  ranging from 100 to 500  $\mu\text{L h}^{-1}$ . Increasing  $Q_{in}$  while keeping  $Q_{out}$  constant, only results in minor increase of the jet velocity, while an increase in  $Q_{out}$  from 100 to 500  $\mu\text{L h}^{-1}$  at a constant  $Q_{in}$  of 20  $\mu\text{L h}^{-1}$  leads to an increased jet velocity of 7.5 to 13.7  $\mu\text{m s}^{-1}$ . By altering these flow ratios, jet diameters range from 6.8 to 20.6  $\mu\text{m}$ , leading to a minimal microgel diameter of 8  $\mu\text{m}$  (Movie provided in the Supporting Information).

To investigate the gelation kinetics and measure the spot size of the laser, single pulses are applied on a pre-polymer solution, which is sandwiched between a glass slide and a stained layer of PDMS (staining as described above). A single pulse produces a gelled imprint of the beam spot with a characteristic width depending on the illumination time  $t_{on}$  and the drive current supplied to the laser (Figure 3e,f). At a current of 80 mA and an illumination time  $t_{on}$  of 2 ms, a spot width of 37.7  $\mu\text{m}$  is obtained, while an illumination time  $t_{on}$  of 100 ms yields a spot width of 444  $\mu\text{m}$ . At a current of 160 mA, gel imprints are realized with illumination times as low as 0.3 ms, demonstrating ultra-fast gelation kinetics. The imprint of the beam spot adapts an elliptical form caused by the highly differing divergence angles for the fast and slow axis of the beam, which is characteristic for diode type lasers (Figure 3f). Furthermore, the gel imprint exhibits remnants of an interference pattern, induced by the refractive index changes from glass to PEG-DA precursor to PDMS (cavity effect). In order to minimize the spot size in our jet gelation system, the major axis of the elliptical beam spot is orientated perpendicular to the channel (Figure 3b,f). The length of the produced rod-shaped microgels is measured and compared to the theoretical length  $l_{theory}$  at a current of 80 mA and flow rates of  $Q_{in}$  20  $\mu\text{L h}^{-1}$  and  $Q_{out}$  200  $\mu\text{L h}^{-1}$  for different  $t_{on}$  and a constant  $t_{off}$  of 20 ms (Figure 3g).  $l_{theory}$  is defined as the sum of the experimental spot width ( $z$ ) and the length  $d$ , representing the distance that a point in the jet travels during  $t_{on}$ . As predicted, the length of the microgels scales with increasing  $t_{on}$ , with accurate predictions for short pulse



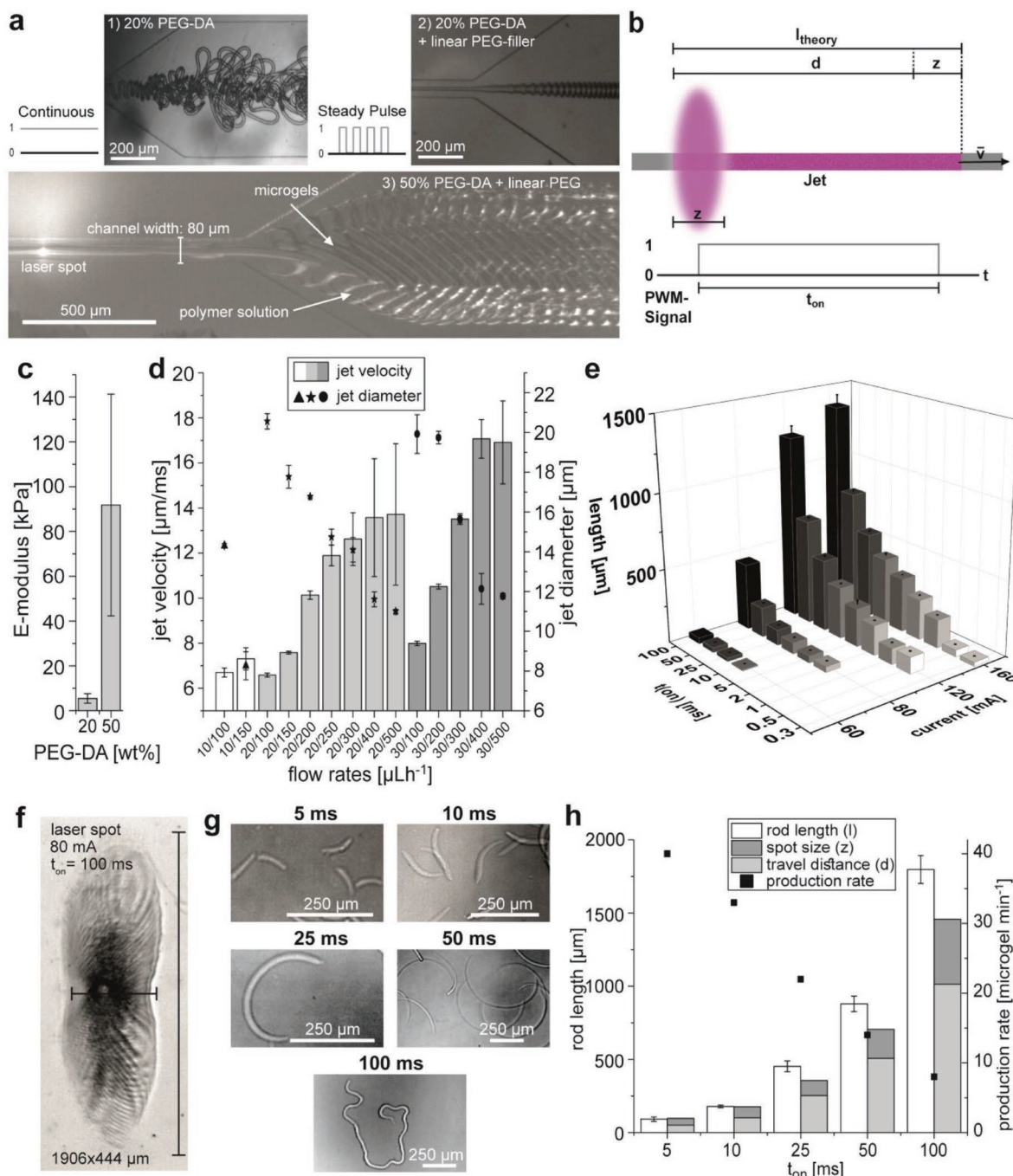


**Figure 3.** Jet gelation is performed with a 405 nm laser diode operating at 45–160 mA in the steady pulse mode to produce microgels with a diameter significantly smaller than the channel diameter. The PDMS layer of the chip is stained in order to absorb the laser light after passing the channel plane. The laser is irradiating the chip from the glass side. The inner phase consists of 20 wt% PEG-DA, 2.4 wt% PEG ( $400,000 \text{ g mol}^{-1}$ ) as filler to increase the viscosity, and 1 wt% LAP. Pure Span80 is used as outer phase. The experiments are repeated at least three times. a) Continuous illumination with the laser results in an endless microgel fiber (image 1, upper panel). Steady pulses yield a characteristic “fishbone” pattern at the onset of the widening output channel (top right and bottom images). b) The theoretical rod length  $l^{\text{theory}}$  is predicted based on the jet velocity  $v$ , the spot width  $z$ , and the pulse duration  $t_{\text{on}}$ . c) Microgel stiffness, depending on the pre-polymer concentration. d) A high-speed camera ( $1000 \text{ pictures s}^{-1}$ ) is connected to a brightfield microscope to track blue latex beads ( $\varnothing = 800 \text{ nm}$ ) dispersed in the inner phase to measure the jet velocity in dependence of the flow rates  $Q_{\text{in}}$  and  $Q_{\text{out}}$ . e) The spot width of the laser is characterized via brightfield microscopy by applying single pulses on a layer of pre-polymer solution, which is squeezed between a glass slide and a colored PDMS sheet. The solution is composed of 20 wt% PEG-DA and 1 wt% LAP, while the thickness mimics the thickness of the jet. f) An exemplary imprint of the laser beam spot is shown for a pulse duration of 100 ms at 80 mA. g) The rod length is adjusted by changing  $t_{\text{on}}$ . The gels are monitored using brightfield microscopy. h) Comparing the experimentally determined rod lengths with  $l^{\text{theory}}$  proves perfect agreement for short  $t_{\text{on}}$  and increasing variances for longer gelation times. The theoretical microgel production rate increases with the frequency (in this case smaller  $t_{\text{on}}$  for constant  $t_{\text{off}}$ ).

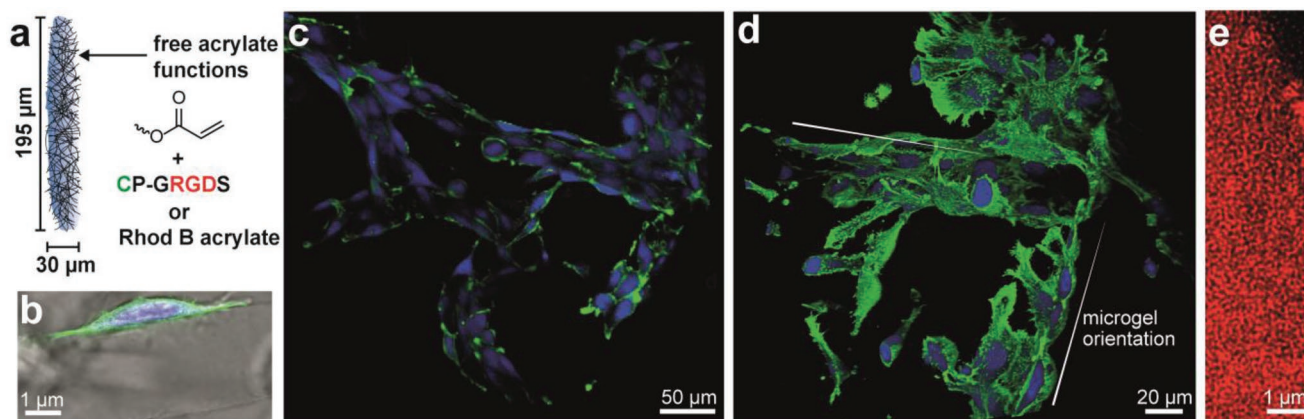


**Figure 4.** The rod-shaped microgels can assemble into 3D structures and support cell growth on their surface. a) Free acrylate groups on the soft microgels are functionalized with cell-adhesive RGD via the thiol of a cysteine. b–d) After 3 days, L929 fibroblasts are stained with phalloidin (green) and 4',6-diamidino-2-phenylindole (blue). b) Cells attach to the surface of the RGD-modified microgels and elongate along the microgel. c) The microgel rods assemble into 3D macroporous structures and are surrounded by a high concentration of cells. d) Higher magnification to demonstrate the lumens where the microgels are located (also see videos in the Supporting Information). Cells wrap around their cylindrical structures. e) Rhodamine B-acrylate is coupled to the microgels to demonstrate the relative large mesh size  $\approx 500$  nm and thus porosity for unhindered nutrient diffusion.

durations but underestimated rod lengths at higher pulse durations (Figure 3h). For instance,  $t_{\text{on}} = 5$  ms yields a rod length of  $91 \mu\text{m}$ , which is close to the theoretically predicted length of  $97 \mu\text{m}$ , while for  $t_{\text{on}} = 100$  ms, the rod length is underestimated by 23%. Possible explanations for this discrepancy may be radical diffusion promoted by the flow dynamics of the jet during irradiation and the fact that at higher laser power or longer  $t_{\text{on}}$ , the area in the spot size where the light intensity is sufficiently high to start the initiation may be increased. For a constant  $t_{\text{off}} = 20$  ms and a varying  $t_{\text{on}}$  from 5 to 100 ms, the theoretical microgel production rate varies from  $40$  to  $8 \text{ s}^{-1}$ , respectively (Figure 3h). To further increase the production rate,  $t_{\text{off}}$  can be reduced to a minimum of 5 ms, resulting in production rates of 100 microgels per second.

Microgel rods produced via in-jet gelation are post-functionalized with a cell adhesive RGD (arginine-glycine-aspartic acid)-derivative (GRGDS-PC) containing a thiol group to bind residual acrylate functions in the microgel (Figure 4a). After RGD modification, the microgels are washed, sterilized, and sedimented, after which fibroblast cells are seeded on top. As demonstrated in Figure 4, microgels assemble into 3D macroporous structures and support cell attachment and growth (Figure 4b,c). While cells wrap around the cylindrical microgel geometry (Figure 4d), larger micron-scale pores in between the rods offer space for cell infiltration, migration, and proliferation, and would likely facilitate blood vessel formation when injected in vivo. Movies of the cell experiments are implemented in the Supporting Information.

In order to monitor the porosity of the material, rhodamine B acrylate is coupled to free acrylate functions in the microgels to enable high-resolution stimulated emission depletion microscopy. The obtained porosity of the jet-produced microgels is compared to the porosity of rod-shaped microgels, previously produced in our laboratory via PRINT, using two different crosslinking chemistries (see Figure S5 in the Supporting Information).<sup>[4,11]</sup> Interestingly, PEG-DA-based in-jet gelation yields microgels with an average pore size of  $510$  nm, which

is nearly five times larger than rods produced via PEG-DA-based PRINT.<sup>[4]</sup> The size difference is even more pronounced in comparison to highly homogenous microgels made via amine/epoxy click chemistry in PRINT.<sup>[11]</sup> We assume that the ultra-fast in-jet segmented gelation produces completely different network structures, which are extremely open and thus very suitable for cell culture. This makes the microgels highly promising biomaterial building blocks to produce injectable, artificial tissue regenerative scaffolds with hierarchical porous character inside and between the microgels.

In summary, a novel microfluidic method is demonstrated to continuously produce anisometric microgels with sub-channel diameters and variable aspect ratio and stiffness. The microgels have diameters that are  $\approx 10$  times smaller than the channel diameter, aspect ratios up to 12.5, elastic moduli down to  $3.9$  kPa, and can be continuously produced at production rates of up to 100 gels per second. Compared to other available fabrication methods of anisometric microgels, PDMS-based microfluidics provides a continuous, reproducible, and user-friendly technique. A laser/UV-LED driver is applied to operate different light sources, such as LEDs and lasers diodes for pulse generation, and induce *on-chip* photopolymerization. Ultra-fast gelation kinetics is observed depending on the pre-polymer concentration, resulting in efficient *on-chip* crosslinking to maintain the anisometric shapes of the microgels. By operating the laser in pulsed mode, alternating segments in the jet are gelled, allowing for high-throughput production of microgel rods. This technology can be applied to produce building blocks for self-assembling microgel systems and 3D injectable, macroporous, directed, and active constructs. Conventional synthetic hydrogels, prepared by crosslinking polymers, result in nanomeshed pores, which do not facilitate cell infiltration and migration in tissue engineering applications. Replacing the nanoscale polymers with microgel rods produced here opens new opportunities to fabricate constructs with defined mechanical and structural properties for in vitro and in vivo operation. Moreover, the novel setup is highly versatile and modular and



therefore exhibits outstanding potential for transfer also in other fields of research and engineering. By linking specific chemical or biological groups, or incorporating nanoparticles, such as gold, iron oxide, carbon nanotubes, or graphene, the microgels become functional and useful for a wide variety of applications, such as bioprinting, actuators, heat and electrical conductance for micro- and nanoelectronics, and medical applications.

## Experimental Section

Experimental materials and methods are provided in the Supporting Information.

## Supporting Information

Supporting Information is available from the Wiley Online Library or from the author.

## Acknowledgements

A.J.D.K. and O.B. contributed equally to this work. This work was supported by the Collaborative Research Center (CRC) grants CRC985 and SFB985 B5 and C3 from DFG (Deutsche Forschungsgemeinschaft), the European Research Council (ERC) under the European Union's Horizon 2020 research and innovation program (ANISOGEL, grant agreement No. 637853) and the European Commission (EUSMI, 731019). This work was performed in part at the Center for Chemical Polymer Technology CPT, which was supported by the EU and the federal state of North Rhine-Westphalia (Grant EFRE 30 00 883 02). The authors wish to thank Dr. Rostislav Vinokur and Sebastian Weiss at DWI for providing technical experience.

## Conflict of Interest

The authors declare no conflict of interest.

## Keywords

anisometric microgels, jet gelation, microfluidics, on-chip gelation, soft microgels

Received: June 10, 2019

Revised: August 22, 2019

Published online: October 17, 2019

- [1] Y. Du, E. Lo, S. Ali, A. Khademhosseini, *Proc. Natl. Acad. Sci. USA* **2008**, *105*, 9522.
- [2] J. J. Crassous, A. M. Mihut, L. K. Mansson, P. Schurtenberger, *Nanoscale* **2015**, *7*, 15971.
- [3] J. J. Crassous, H. Dietsch, P. Pfeleiderer, V. Malik, A. Diaz, L. A. Hirshi, M. Drechsler, P. Schurtenberger, *Soft Matter* **2012**, *8*, 3538.
- [4] A. J. D. Krüger, J. Köhler, S. Cichosz, J. C. Rose, D. B. Gehlen, T. Haraszti, M. Möller, L. De Laporte, *Chem. Commun.* **2018**, *54*, 6943.
- [5] W. Li, L. Zhang, X. Ge, B. Xu, W. Zhang, L. Qu, C.-H. Choi, J. Xu, A. Zhang, H. Lee, D. A. Weitz, *Chem. Soc. Rev.* **2018**, *47*, 5646.
- [6] L. Tao, W. Hu, Y. Liu, G. Huang, B. D. Sumer, J. Gao, *Exp. Biol. Med.* **2011**, *236*, 20.
- [7] S. E. A. Gratton, P. A. Ropp, P. D. Pohlhaus, J. C. Luft, V. J. Madden, M. E. Napier, J. M. DeSimone, *Proc. Natl. Acad. Sci. USA* **2008**, *105*, 11613.
- [8] W. Yang, H. Yu, G. Li, Y. Wang, L. Liu, *Small* **2017**, *13*, 1602769.
- [9] D. R. Griffin, W. M. Weaver, P. O. Scumpia, D. Di Carlo, T. Segura, *Nat. Mater.* **2015**, *14*, 737.
- [10] S. Ma, N. Mukherjee, E. Mikhailova, H. Bayley, *Adv. Biosyst.* **2017**, *1*, 1700075.
- [11] J. C. Rose, M. Cámara-Torres, K. Rahimi, J. Köhler, M. Möller, L. De Laporte, *Nano Lett.* **2017**, *17*, 3782.
- [12] A. Omidinia-Anarkoli, S. Boesveld, U. Tuvshindorj, J. C. Rose, T. Haraszti, L. De Laporte, *Small* **2017**, *13*, 1702207.
- [13] J. C. Rose, D. B. Gehlen, T. Haraszti, J. Köhler, C. J. Licht, L. De Laporte, *Biomaterials* **2018**, *163*, 128.
- [14] A. Mourran, H. Zhang, R. Vinokur, M. Möller, *Adv. Mater.* **2017**, *29*, 1604825.
- [15] H. Zhang, A. Mourran, M. Möller, *Nano Lett.* **2017**, *17*, 2010.
- [16] L. P. B. Guertzoni, J. C. Rose, D. B. Gehlen, A. Jans, T. Haraszti, M. Wessling, A. J. C. Kuehne, L. De Laporte, *Small* **2019**, *15*, 1900692.
- [17] J. P. Rolland, B. W. Maynor, L. E. Euliss, A. E. Exner, G. M. Denison, J. M. DeSimone, *J. Am. Chem. Soc.* **2005**, *127*, 10096.
- [18] S. E. A. Gratton, P. D. Pohlhaus, J. Lee, J. Guo, M. J. Cho, J. M. DeSimone, *J. Controlled Release* **2007**, *121*, 10.
- [19] L. C. Glangchai, M. Caldorera-Moore, L. Shi, K. Roy, *J. Controlled Release* **2008**, *125*, 263.
- [20] L. E. Euliss, J. A. DuPont, S. Gratton, J. DeSimone, *Chem. Soc. Rev.* **2006**, *35*, 1095.
- [21] J. A. Champion, Y. K. Katare, S. Mitragotri, *Proc. Natl. Acad. Sci. USA* **2007**, *104*, 11901.
- [22] J. A. Champion, Y. K. Katare, S. Mitragotri, *J. Controlled Release* **2007**, *121*, 3.
- [23] D. Dendukuri, K. Tsoi, T. A. Hatton, P. S. Doyle, *Langmuir* **2005**, *21*, 2113.
- [24] a) S. Xu, Z. Nie, M. Seo, P. Lewis, E. Kumacheva, H. A. Stone, P. Garstecki, D. B. Weibel, I. Gitlin, G. M. Whitesides, *Angew. Chem., Int. Ed.* **2005**, *44*, 724; b) S. Xu, Z. Nie, M. Seo, P. Lewis, E. Kumacheva, H. A. Stone, P. Garstecki, D. B. Weibel, I. Gitlin, G. M. Whitesides, *Angew. Chem.* **2005**, *117*, 734.
- [25] R. M. Erb, D. Obrist, P. W. Chen, J. Studer, A. R. Studart, *Soft Matter* **2011**, *7*, 8757.
- [26] K. Liu, H.-J. Ding, J. Liu, Y. Chen, X.-Z. Zhao, *Langmuir* **2006**, *22*, 9453.
- [27] S. Duraiswamy, S. A. Khan, *Small* **2009**, *5*, 2828.
- [28] M. Yamada, S. Sugaya, Y. Naganuma, M. Seki, *Soft Matter* **2012**, *8*, 3122.
- [29] J. K. Nunes, K. Sadlej, J. I. Tam, H. A. Stone, *Lab Chip* **2012**, *12*, 2301.
- [30] D. Dendukuri, P. S. Doyle, *Adv. Mater.* **2009**, *21*, 4071.
- [31] D. Dendukuri, D. C. Pregibon, J. Collins, T. A. Hatton, P. S. Doyle, *Nat. Mater.* **2006**, *5*, 365.
- [32] D. Dendukuri, S. S. Gu, D. C. Pregibon, T. A. Hatton, P. S. Doyle, *Lab Chip* **2007**, *7*, 818.
- [33] a) J.-H. Jang, D. Dendukuri, T. A. Hatton, E. L. Thomas, P. S. Doyle, *Angew. Chem., Int. Ed.* **2007**, *46*, 9027; b) J.-H. Jang, D. Dendukuri, T. A. Hatton, E. L. Thomas, P. S. Doyle, *Angew. Chem.* **2007**, *119*, 9185.
- [34] P. Panda, S. Ali, E. Lo, B. G. Chung, T. A. Hatton, A. Khademhosseini, P. S. Doyle, *Lab Chip* **2008**, *8*, 1056.
- [35] D. K. Hwang, J. Oakey, M. Toner, J. A. Arthur, K. S. Anseth, S. Lee, A. Zeiger, K. J. Van Vliet, P. S. Doyle, *J. Am. Chem. Soc.* **2009**, *131*, 4499.
- [36] G. C. Le Goff, J. Lee, A. Gupta, W. A. Hill, P. S. Doyle, *Adv. Sci.* **2015**, *2*, 1500149.
- [37] T. Cubaud, T. G. Mason, *Phys. Fluids* **2008**, *20*, 053302.
- [38] Y. Jun, E. Kang, S. Chae, S.-H. Lee, *Lab Chip* **2014**, *14*, 2145.
- [39] B. D. Fairbanks, M. P. Schwartz, C. N. Bowman, K. S. Anseth, *Biomater.* **2009**, *30*, 6702.